



Regular Article

Synthesis of magnetic ZnO/ZnFe₂O₄ by a microwave combustion method, and its high rate of adsorption of methylene blue



Jing Feng*, Yuting Wang, Linyi Zou, Bowen Li, Xiaofeng He, Yueming Ren, Yanzhuo Lv, Zhuangjun Fan*

Key Laboratory of Superlight Materials & Surface Technology of Ministry of Education, Harbin Engineering University, Harbin 150001, PR China

ARTICLE INFO

Article history:

Received 12 July 2014

Accepted 9 October 2014

Available online 18 October 2014

Keywords:

Magnetic properties

Adsorption

ZnO

ZnFe₂O₄

Methylene blue

ABSTRACT

The magnetic ZnO/ZnFe₂O₄ particles have been synthesized by a microwave combustion method using NaAc as fuel. The as-obtained ZnO/ZnFe₂O₄ was characterized and applied for the removal of methylene blue (MB) from aqueous solution in the batch system. The ZnO/ZnFe₂O₄ particles display larger S_{BET} and smaller size with increase of NaAc dosage. Because a certain amount of gas is generated during NaAc decomposing and the gas prevent the particles from growing larger. More interestingly, even at neutral pH value, the ZnO/ZnFe₂O₄ obtained with 24 mL NaAc shows high-rate adsorption properties with the MB removal efficiency up to 90% in 0.5 min and a maximum adsorption capacity of 37.27 mg/g.

© 2014 Elsevier Inc. All rights reserved.

1. Introduction

Adsorption is a promising way to remove organic dyes [1–4], but the difficult separation of sorbents from water hinders the application. Magnetic separation is an effective technique to separate sorbents from wastewater by applying an external magnetic field [5]. Ferrite oxides MFe₂O₄ (M = Zn, Fe, Co, Mn, etc.) are always used as magnetic carrier due to their ferromagnetic property, such as Fe₃O₄/grapheme [6], ferrite/carbon nanotube [7], activated carbon/ferrite [8] and TiO₂/ferrite [9–11]. However, a composite adsorbent containing ferrite often shows lower S_{BET} and adsorption capacity. For example, the S_{BET} of activated carbon [12] and activated carbon/CoFe₂O₄ [8] decreases from 909 m²/g to 463 m²/g and the adsorption capacity for malachite green decrease from 329.49 mg/g to 89.29 mg/g. Nevertheless, ferrite oxide also shows excellent adsorption as long as it has high surface area [13–15]. Coupling high surface area materials with spinel ferrite is an effective way to improve surface area and adsorption capacity. ZnO is a high surface area oxide and it is easily synthesized with various morphologies [16,17]. Hence, ZnO incorporated with ZnFe₂O₄ may exhibit not only high adsorption capacity but also magnetic separation.

Ferrite can be synthesized by microwave combustion method, in which the raw materials can directly absorb microwave energy and the reaction completes in a few minutes [18,19]. The microwave energy affects size and shape of particles. For example,

Zn_xNi_{1-x}Fe₂O₄ nanocrystallines [20], ZnO nanoparticles [21] and NiAl₂O₄ nanoparticles [22] have been synthesized by microwave assisted combustion method with uniform and small size. In a microwave combustion process, the organic fuel is used as both combustion fuel and complex agent, and it can determine the morphology and phase formation of final product. Different organic fuels, such as glycine urea [23] and sodium acetate [24], are used to fabricate nano-size ferrite by microwave combustion method. Generally, both nature of fuel and ratio of fuel to oxidant are related to flame temperature, which directly affects the surface area, size-distribution and agglomeration of the final particles. Costa et al. [25] synthesized Ni–Zn–Sm ferrites by microwaves combustion reaction using urea, glycine and mixture of urea/glycine and they found the relation between different fuel and the phase formation. So far, there is rare study about the effect of the ratio between fuel and nitrate on crystalline phase, particle size and property. Herein, we introduce ZnO into ZnFe₂O₄ in order to improve the surface area and adsorption capacity. And the effects of the fuel (NaAc) dosage on morphologies and adsorption properties of ZnO/ZnFe₂O₄ synthesized by microwave combustion method have also been studied.

2. Experimental

2.1. Sample preparations

ZnO/ZnFe₂O₄ was synthesized by microwave combustion method. Firstly, 1.7848 g Zn(NO₃)₂·6H₂O (AR), 4.0400 g Fe(NO₃)₃·9H₂O (AR) and 0.5 g polyethylene glycol (AR) were mixed with

* Corresponding authors. Fax: +86 451 82533026.

E-mail addresses: fengjing@hrbeu.edu.cn (J. Feng), fanzhj666@163.com (Z. Fan).

15 mL distilled water under vigorous stirring. Then, 24 mL sodium acetate (NaAc, AR) solution (0.5 g/mL) was dripped into solution. The mix solution was placed into a domestic microwave oven and promulgated at 120 W for 5 min and 700 W for 10 min. Lastly, the solid powder (named ZFO24) was washed with water and ethanol for several times, and dried at 60 °C for 24 h. To investigate the function of dosage NaAc, the other samples were prepared by using a similar route with the NaAc solution dosages of 6 mL, 10 mL, 20 mL and 28 mL, and named as ZFO6, ZFO10, ZFO20 and ZFO28, respectively.

2.2. Characterizations

The samples were characterized by X-ray diffraction (XRD, Rigaku/ITR-III with Cu K α radiation), scanning electron microscopy (SEM, SIRION/HITACHI/S-4800), high resolution transmission electron microscopy (HRTEM, JEOL/JEM-2010), vibrating sample magnetometer (VSM, JDM-14D). The surface area was determined by BET measurements (SSA4200). The concentration of MB is analyzed by using 721 UV-Visible Spectrophotometer (China) with the maximum absorption wavelength of MB at 655 nm.

2.3. Adsorption experiments

All ZnO/ZnFe₂O₄ adsorbents (80 mg) and MB solution (100 mL) were added into conical flask to investigate the adsorption of MB in a dark chamber. The effects of pH (3–11) and initial dye concentration on adsorption properties were determined. The adsorption isotherm was tested over the MB concentration range of 5–100 mg/L at pH 7. The concentration of MB in the solution was analyzed by standard methods. Adsorption capacity was calculated according to Eqs. (1) and (2):

$$q_e = \frac{(C_0 - C_e)V}{W} \quad (1)$$

$$E_t = \frac{C_0 - C_t}{C_0} \times 100\% \quad (2)$$

where q_e (mg/g) is adsorption capacity, C_0 (mg/L) and C_e (mg/L) are initial and equilibrated MB concentrations, respectively, V (L) is the volume of added solution and W (g) is the mass of the adsorbent (dry).

3. Results and discussion

XRD patterns of ZnO/ZnFe₂O₄ are shown in Fig. 1. All detectable peaks consist with the standard data of ZnFe₂O₄ (JCPDS22-1012) and ZnO (JCPDS36-1451) well. And the intensity of ZnO diffraction peaks obviously increases with increasing dosage of NaAc solution.

Fig. 2 and Table 1 reveal that the NaAc dosage obviously affects their morphologies and BET surface areas (S_{BET}) of ZnO/ZnFe₂O₄.

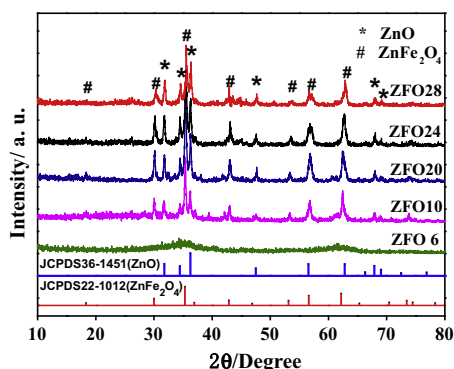


Fig. 1. XRD patterns of ZnO/ZnFe₂O₄.

The ZnO/ZnFe₂O₄ particles display smaller particle size and higher S_{BET} with the increase of NaAc dosage. Among all samples, ZFO28 exhibits the maximum S_{BET} of 94.47 m²/g and minimum particle size of 23–54 nm. Fig. 2g shows that ZnO exhibits fiber-like structure synthesized by using a similar route. The special morphology of ZnO is closely related with their small particles and high specific surface area of ZnO/ZnFe₂O₄ compounds. The HRTEM image (Fig. 2i) exhibits two types of lattice fringes. The distance between one set of fringes is 0.289 nm, which is close to the (100) plane of Wurtzite structural ZnO with 0.281 nm. The other set of fringes with distance of 0.478 nm is corresponded to the (111) plane of spinel structure ZnFe₂O₄ with 0.487 nm. Moreover, the size of ZFO24 after adsorption becomes smaller than before (Fig. 2(d) and (f)).

In the starting solution, NaAc ionizes into Na⁺ and –COOCH₃ group, and the –COOCH₃ group can easily complex with the metal ions Zn²⁺ and Fe³⁺ and generate Fe(COOCH₃)₃ and Zn(COOCH₃)₂ [24]. During the microwave process, high temperature can speed up the decomposition of Fe(COOCH₃)₃ and Zn(COOCH₃)₂ that generates a mass of gas. The escaping gas favors the formation of smaller particles during the heat-treatment. More NaAc dosage can generate more gas that might prevent the particles from growing larger. On the other hands, the combustion reaction finishes in a very short time during a microwave combustion process. Therefore, there is almost no time for grain growth, which also results in fine particles and high specific surface area of ZnO/ZnFe₂O₄. In our work, the S_{BET} increases for 59.520 m²/g of ZFO6 to 94.466 m²/g of ZFO28. The relatively high specific surface area will benefit to the adsorption activity.

Excellent magnetic performance plays a key role in magnetic separation. Magnetic hysteresis loops of all samples at room temperature are shown in Fig. 3. The ZFO6 shows paramagnetism because the ZnFe₂O₄ phase fails to obtain. The ZFO10 exhibits the highest saturation magnetization (M_s) of 55.83 emu/g, which is higher than previously reported ZnO/ZnFe₂O₄ hollow nanospheres (10.10 emu/g) [26]. The magnetization decreases with the increase of NaAc dosage. The decrease tendency of M_s is consistent with the reduction of particle size of the investigated solids [24].

3.1. Effect of NaAc dosage on adsorption properties

The effect of NaAc dosage on the removal efficiency of MB (10 mg/L) is shown in Fig. 4. With the increase of NaAc dosage, the ZnO/ZnFe₂O₄ particles display better removal efficiency. This can be attributed to the ZnO/ZnFe₂O₄ particles becoming more uniform distributed, smaller particle size and higher S_{BET} (Table 1). Therefore, the ZFO6, ZFO10 and ZFO16 samples show low removal efficiency while the ZFO20, ZFO24 and ZFO28 samples show high adsorption rate for removing MB and the removal efficiencies reach up to 90% in 0.5 min. The adsorption rate is much faster than other reported data [27,28]. Therefore, ZnO/ZnFe₂O₄ is a promising high-rate sorbent for removing industrial organic dyes. The supporting video illustrates the processes of quick adsorption and magnetic separation for the sample ZFO24.

3.2. Effect of pH on adsorption

The value of pH is an important parameter affecting the adsorption. The effect of pH (3–11) on the removal of MB (10 mg/L) is shown in Fig. 5. The removal efficiency is the lowest at pH 3, and the minimum value is 83%. The removal efficiencies at equilibrium state are higher than 99% in the wide range of pH 4–11. Furthermore, the removal efficiencies of MB on ZFO24 reach 90% within 0.5 min in pH 7–11. It is supposed that coulomb interaction plays an important role in the adsorption of MB onto ZnO/ZnFe₂O₄. Thus, pH 7 is selected as optimum pH for the other experiments.

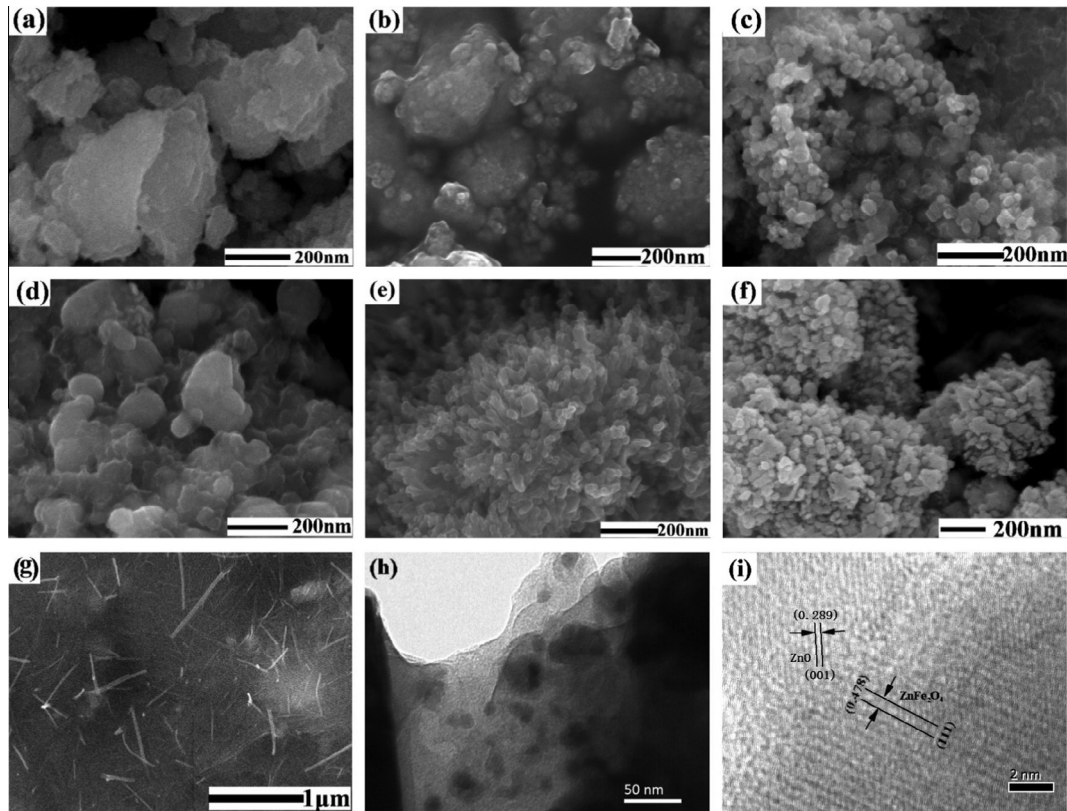


Fig. 2. SEM images of a: ZFO6, b: ZFO10, c: ZFO20, d: ZFO24, e: ZFO28, f: the ZFO24 after adsorbing MB, g: ZnO made by the same condition; and (h–i) TEM images of ZFO24.

Table 1
BET surface areas (S_{BET}) of ZnO/ZnFe₂O₄.

Samples	ZFO10	ZFO20	ZFO24	ZFO28
S_{BET} (m ² /g)	59.520	68.003	89.054	94.466
Particle size (nm)	102–208	32–60	30–81	23–54

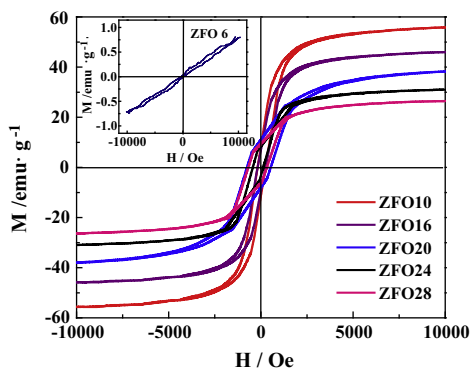


Fig. 3. Magnetic hysteresis loops of ZnO/ZnFe₂O₄ at room temperature.

3.3. Adsorption kinetics

Fig. 6a shows the adsorption kinetics of ZnO/ZnFe₂O₄ for MB removal. The adsorption capacity increases rapidly within 1 min, and the equilibrium time is about 5 min. In order to investigate the mechanism of adsorption kinetics, pseudo-first-order and pseudo-second-order kinetics models are applied to interpret adsorption dynamics. The pseudo-first-order kinetic model (Eq. (3)) and pseudo-second-order model (Eq. (4)) are shown as the following equations:

$$\log(q_e - q_t) = \log q_e - \left(\frac{k_1}{2.303}\right)t \quad (3)$$

$$\frac{t}{q_t} = \frac{1}{k_2 q_e^2} + \frac{1}{q_e} t \quad (4)$$

where q_e and q_t (mg/g) are the amounts of MB adsorbed onto adsorbent at equilibrium and any time t (min), respectively. k_1 (h⁻¹) is the first-order rate constant and k_2 ((g/mg)/min) is the second-order rate constant. Plotting the experiment data in the form of $\log(q_e - q_t)$ versus t or t/q_t against t (min) a straight line would be obtained if the kinetic model is a suitable expression.

The linear regression is presented in Fig. 6(b and c) and the parameters are listed in Table 2. The pseudo-second-order adsorption mechanism is predominant for this adsorbent system. Also, the theoretical value $q_{e,\text{cal}}$ obtained by pseudo-second-order (12.89 mg/g) agrees experimental value $q_{e,\text{exp}}$ (12.85 mg/g) well. It can be concluded that the overall rate of MB adsorption process is controlled by the chemical reaction [29].

3.4. Adsorption isotherm

Langmuir adsorption isotherm and Freundlich model are used to describe the adsorption of MB onto ZnO/ZnFe₂O₄ at room temperature. The adsorption capacities of ferrites ZnO/ZnFe₂O₄ are calculated by using Langmuir (Eq. (5)) and Freundlich (Eq. (6)) models, expressed by the following equations.

$$q_e = \frac{q_m K_L C_e}{1 + K_L C_e} \quad (5)$$

$$q_e = K_F C_e^{\frac{1}{n}} \quad (6)$$

where q_e (mg/g) is the amount of adsorbate adsorbed at equilibrium, q_m (mg/g) is the maximum adsorption capacity of the adsorbate by the sorbent, K_L (L/mg) is the Langmuir adsorption constant

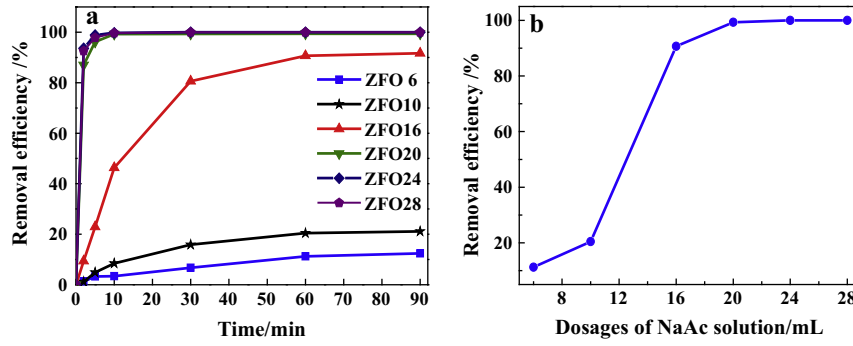


Fig. 4. Effects of NaAc dosage on the removal efficiency of MB.

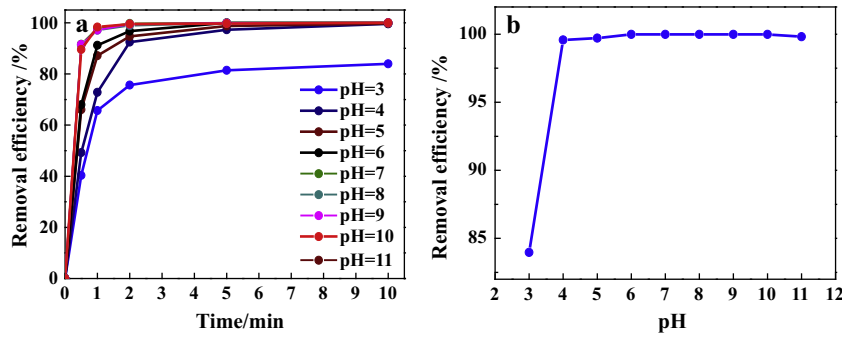


Fig. 5. Effects of pH on the removal efficiency of MB for ZFO24.

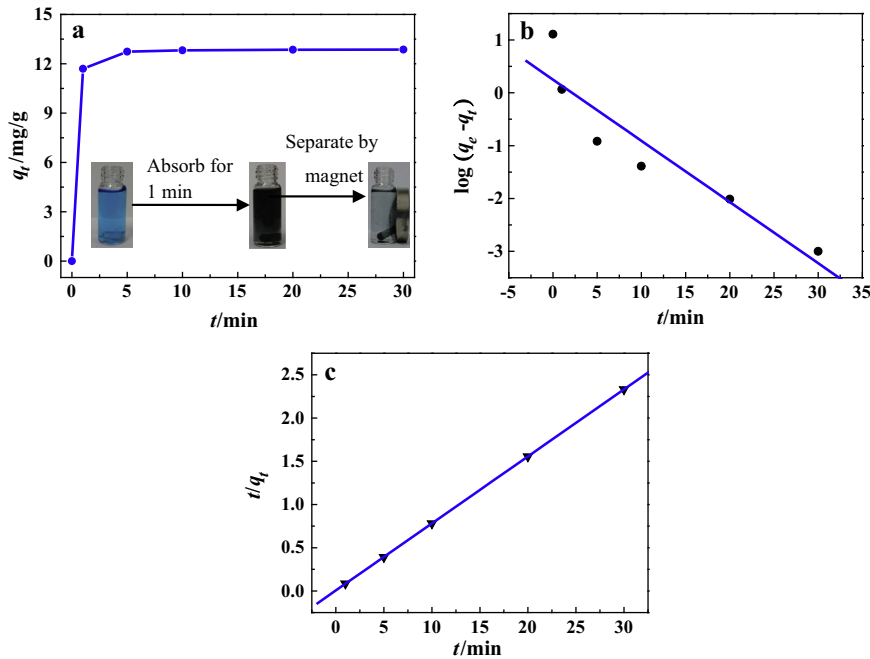


Fig. 6. (a) Adsorption kinetics of ZFO24 for MB, (b) the fitting line of pseudo-first-order, and (c) the fitting line of pseudo-second-order.

Table 2

Kinetic parameters for adsorption MB onto ZFO24.

$q_{e,exp}$ (mg/g)	Pseudo-first-order			Pseudo-second-order			
	k_1 (min^{-1})	$q_{e,cal}$ (mg/g)	R^2	k_2 ($\text{g min}^{-1} \text{min}^{-1}$)	$q_{e,cal}$ (mg/g)	H ($\text{mg g}^{-1} \text{min}^{-1}$)	R^2
12.85	0.267	1.28	0.872	1.018	12.89	165.1	1

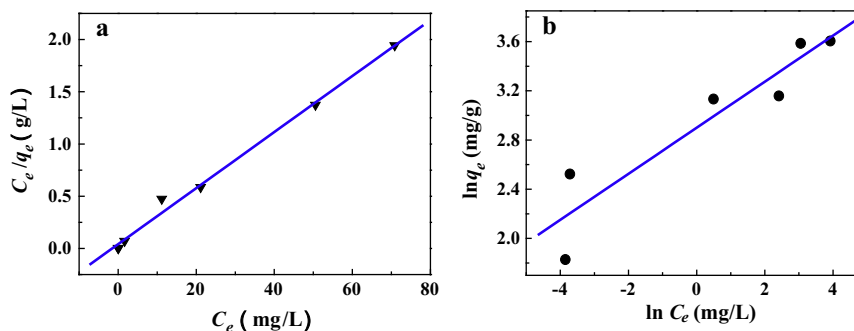


Fig. 7. Linear isotherm plots of Langmuir (a) and Freundlich (b) isotherm of MB onto ZFO24.

Table 3

Isotherm constants for MB adsorption onto ZFO24.

Langmuir model			Freundlich model			
q_m (mg/g)	K_L (L/mg)	R_L	R^2	K_F (mg/g (mg/L) $^{1/n}$)	$1/n$	R^2
37.272	0.655	0–1	0.9935	18.18	0.18723	0.8739

related to the free energy of adsorption, K_F and n are the Freundlich constants related respectively to adsorption capacity and adsorption intensity.

Fig. 7a and Table 3 shows the results of linear fitting in Langmuir isotherm for ZFO24. The correlation coefficient (R^2) is 0.9935, indicating that the Langmuir adsorption model is successfully applied in this affinity adsorbent system Fig. 7b. The value of $1/n$ is in the range of 0.1–1, indicating the favorable removal conditions. However, the correlation coefficients reflects that the experimental data do not fit with the Freundlich model well.

We can assume that all the binding sites on the sorbent are free sites and ready to accept the adsorbate from solution. The affinity between MB and ZFO24 can be predicted using Langmuir dimensionless separation factor R_L given by the relation as Eq. (7):

$$R_L = \frac{1}{1 + K_L C_0} \quad (7)$$

where C_0 (mg/L) is the initial MB concentration. The values of R_L in our test are all $0 < R_L < 1$ indicated a favorable adsorption [30].

4. Conclusions

Magnetic ZnO/ZnFe₂O₄ particles synthesized via a microwave combustion method show high adsorption capacity and high adsorption rate for the removal of MB. The results suggest that the fuel content has a significant influence on the morphologies and the adsorption capacity in microwave combustion process. With the increase in NaAc dosage, the size of the ZnO/ZnFe₂O₄ particles decreases, resulting in higher S_{BET} and higher removal capacity. The removal efficiencies of ZFO20, ZF24, ZF28 can reach up to 90% within 0.5 min at pH 7. Therefore, we consider that the ZnO/ZnFe₂O₄ sorbent can be used as a promising, effective and magnetic separation adsorbent for the removal organic dye from wastewater.

Acknowledgments

We appreciate the financial supports from the National Natural Science Foundation of China (NSFC) (21301038, 51108111, 21203040), the Natural Science Foundation of Heilongjiang Province of China (B201201), and Fundamental Research Funds for the Central Universities and Program for New Century Excellent Talents in University (NCET-10-0050).

Appendix A. Supplementary material

Supplementary data associated with this article can be found, in the online version, at <http://dx.doi.org/10.1016/j.jcis.2014.10.009>.

References

- [1] A.H. Karim, A.A. Jalil, S. Triwahyono, S.M. Sidik, N.H.N. Kamarudin, R. Jusoh, N.W.C. Jusoh, B.H. Hameed, J. Colloid Interface Sci. 386 (2012) 307–314.
- [2] R. Guo, L.D. Wilson, J. Colloid Interface Sci. 388 (2012) 225–234.
- [3] G.F. Malash, M.I. El-Khaiary, J. Colloid Interface Sci. 348 (2010) 537–545.
- [4] S.T. Yang, S. Chen, Y. Chang, A. Cao, Y. Liu, H. Wang, J. Colloid Interface Sci. 359 (2011) 24–29.
- [5] G.S. Zhang, J.H. Qu, H.J. Liu, A.T. Cooper, R.C. Wu, Chemosphere 68 (2007) 1058–1066.
- [6] F. He, J. Fan, D. Ma, L. Zhang, C. Leung, H.L. Chan, Carbon 48 (2010) 3139–3144.
- [7] C.L. Chen, X.K. Wang, M. Nnagatsu, Environ. Sci. Technol. 43 (2009) 2362–2367.
- [8] L. Ai, H. Huang, Z. Chen, X. Wei, J. Jiang, Chem. Eng. J. 156 (2010) 243–249.
- [9] S.H. Xuan, W.Q. Jiang, X.L. Gong, Y. Hu, Z.Y. Chen, J. Phys. Chem. C 113 (2009) 553–558.
- [10] Y.P. Fu, W.K. Chang, H.C. Wang, C.W. Liu, C.H. Lin, J. Mater. Res. 25 (2010) 134–140.
- [11] S.H. Xu, W.F. Shangguan, J. Yuan, M.X. Chen, J.W. Shi, Appl. Catal. B 71 (2007) 177–184.
- [12] M.A. Ahmad, R. Alroz, Chem. Eng. J. 171 (2011) 510–516.
- [13] R. Rahimi, H. Kerdari, M. Rabbani, M. Shafiee, Desalination 280 (2011) 412–418.
- [14] S. Xuan, F. Wang, Y.J. Wang, Y. Jimmy, K. Leung, J. Mater. Chem. 20 (2010) 5086–5094.
- [15] W. Konicki, D. Sibera, E. Mijowska, Z. Lendzion-Bieluń, U. Narkiewicz, J. Colloid Interface Sci. 398 (2013) 152–160.
- [16] Y.W. Heo, D.P. Norton, L.C. Tien, Y. Kwon, B.S. Kang, F. Ren, S.J. Pearton, J.R. LaRoche, Mat. Sci. Eng. R 47 (2004) 1–47.
- [17] H. Zhang, D. Yang, X. Ma, Y. Ji, J. Xu, D. Que, Nanotechnology 15 (2004) 622–626.
- [18] P. Yadoji, R. Peelamedu, D. Agrawal, R. Roy, Mater. Sci. Eng. B 98 (2003) 269–278.
- [19] Y. Köseoglu, A. Baykal, F. Gözüak, H. Kavas, Polyhedron 28 (2009) 2887–2892.
- [20] M. Sertkol, Y. Köseoglu, A. Baykal, H. Kavas, A. Bozkurt, M.S. Toprak, J. Alloys Compd. 486 (2009) 325–329.
- [21] T.T. Ha, T.D. Canh, N.V. Tuyen, ISRN Nanotechnol. 2013 (2013) 7.
- [22] C. Ragupathi, J.J. Vijaya, L.J. Kennedy, Mater. Sci. Eng. B 184 (2014) 18–25.
- [23] A. Manikandan, L.J. Kennedy, M. Bououdina, J.J. Vijaya, J. Magn. Magn. Mater. 349 (2014) 249–258.
- [24] S. Farhadi, M. Zaidi, J. Mol. Catal. A: Chem. 299 (2009) 18–25.
- [25] A.C.F.M. Costa, D.A. Vieira, V.J. Silva, V.C.S. Diniz, R.H.G.A. Kiminami, L. Gama, J. Alloys Compd. 483 (2009) 37–39.
- [26] H. Qian, Y. Hu, Z. Li, X. Yang, L. Li, X. Zhang, R. Xu, J. Phys. Chem. C 114 (2010) 17455–17459.
- [27] M. Dong, Q. Lin, D. Chen, X. Fu, M. Wang, Q. Wu, X. Chen, S. Li, RSC Adv. 3 (2013) 11628–11633.
- [28] R. Wu, J. Qu, H. He, Y. Yu, Appl. Catal., B 48 (2004) 49–56.
- [29] X. Hou, J. Feng, Y. Ren, Z. Fan, M. Zhang, Colloids Surf. A 363 (2010) 1–7.
- [30] Benhammou, A. Yaacoubi, L. Nibou, B. Tanouti, J. Colloid Interface Sci. 282 (2005) 320–324.